PCCP

COMMUNICATION

View Article Online
View Journal | View Issue

Cite this: *Phys. Chem. Chem. Phys.*, 2017, **19**, 7476

Received 14th December 2016,
Accepted 16th February 2017

DOI: 10.1039/c6cp08522a

rsc.li/pccp

An insight into methanol oxidation mechanisms on $RuO_2(100)$ under an aqueous environment by DFT calculations†

Tian Sheng,*[a] Jin-Yu Ye,[a] Wen-Feng Lin[b] and Shi-Gang Sun*[a]

In this work, we have studied methanol oxidation mechanisms on $RuO_2(100)$ by using density functional theory (DFT) calculations and *ab initio* molecular dynamics (MD) simulations with some explicit interfacial water molecules. The overall mechanisms are identified as: $CH_3OH^* \rightarrow CH_3O^* \rightarrow HCHO^* \rightarrow HCH(OH)_2^* \rightarrow HCHOOH^* \rightarrow HCOOH^* \rightarrow$ mono-$HCOO^* \rightarrow CO_2^*$, without CO formation. This study provides a theoretical insight into C1 molecule oxidation mechanisms at atomic levels on metal oxide surfaces under an aqueous environment.

The electrooxidation of alcohol has been the subject of numerous studies for its potential application in fuel cells over the past decades. Liquid methanol has many advantages in safety and transportation and a high energy density as fuels in direct methanol fuel cells (DMFCs).[1] The equilibrium potential in methanol oxidation to CO_2 with the release of six electrons ($CH_3OH + H_2O \rightarrow CO_2 + 6H^+ + 6e^-$) is 0.02 V *vs.* (SHE). To date, platinum still remains the central catalyst in fuel cells, although the CO poisoning issue affects its efficiency seriously.[1–3] Experiments have found that ruthenium is a critical additive for enhancing the activity. Binary PtRu catalysts have shown the highest activity towards methanol oxidation. A bi-functional mechanism was proposed for interpreting the promoting roles of Ru because it can provide oxygen-containing species derived from water dissociation at remarkably lower potentials than pure platinum, and thus CO can be converted into CO_2.[4–8]

Ru is a versatile catalyst in heterogeneous catalysis and electrocatalysis.[9,10] The electrochemical behavior of the Ru single-crystal plane, and the chemistry of small organic molecules has been investigated.[11–15] The surface oxidation states, *i.e.*, (2×2)-O and (1×1)-O were identified over a potential range on Ru(0001).[11–15] No oxidation of methanol is observed at potentials below 0.8 V, suggesting that the surface oxides block the Ru(0001) physically for methanol adsorption. However, at higher potentials, significant oxidation of methanol to CO_2 in acid solution and to bicarbonate and formate in alkaline solution, was observed, which was attributed to the formation of an active $RuO_2(100)$ phase on Ru(0001).[11–15] Wang *et al.* also found that $RuO_2(100)$ was more active than Ru(0001) in CO oxidation.[16] In comparison with the most stable $RuO_2(110)$ surface,[17–19] the $RuO_2(100)$ with the higher surface energy was less investigated in the literature.

Electrocatalysis occurring at electrolyte/electrode interfaces is apparently more complicated than heterogeneous catalysis at gas/solid interfaces. Although some knowledge from heterogeneous catalysis can be transferred to electrocatalysis due to their similarities, the differences have so far mostly been neglected or underestimated. Some studies have been carried out theoretically towards the establishment of reaction mechanisms for methanol oxidation and a lot of surfaces have been studied by first principles calculations.[18–24] Results obtained at the gas/solid interfaces are not very convincing, since behaviors of interfacial water are crucial towards understanding the electrocatalysis chemistry. From the simulations performed in an aqueous interfacial model with explicit water molecules, we may learn a great deal about electrocatalysis at the atomic scale than without them.[25–33] Some results have shown that the presence of aqueous solution has a great impact on mechanisms and energetics of surface reactions.

Herein, in order to reveal the inherent catalytic activity of the $RuO_2(100)$ surface for methanol oxidation, we have investigated the reaction mechanisms in the presence of explicit interfacial water molecules within a DFT framework. An indirect C–H bond breaking mechanism is revealed in which the C–H bond breaking takes place after the O–H bond is broken. A series of reactive intermediates are identified and the presence of water molecules is found to have an important role in formic acid oxidation to CO_2. We anticipate that this work would be of benefit for the further study of small organic molecules reactions in Ru/RuO_2 systems and on other metal oxide surfaces.

The electronic structure calculations were performed using Perdew–Burke–Ernzerh (PBE) generalized gradient approximation

[a] *Collaborative Innovation Centre of Chemistry for Energy Materials, State Key Laboratory of Physical Chemistry of Solid Surfaces, Xiamen University, Xiamen, 361005, China. E-mail: tsheng@xmu.edu.cn, sgsun@xmu.edu.cn*
[b] *Department of Chemical Engineering, Loughborough University, Loughborough, Leicestershire, LE11 3TU, UK*

† Electronic supplementary information (ESI) available. See DOI: 10.1039/c6cp08522a

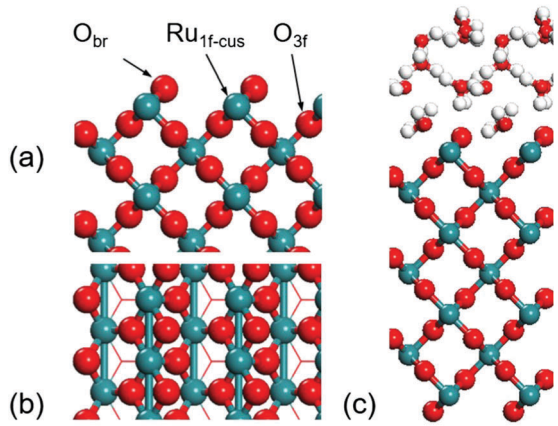

Fig. 1 Side (a) and top (b) views of the $RuO_2(100)$ surface. (c) Model of the aqueous interface. Green: Ru; red: O; white: H. (The same colors are used in the paper.)

(GGA) exchange–correlation functional in Vienna Ab-initio Simulation Package (VASP). The core electron interaction was described by projector-augmented-wave (PAW) pseudopotentials.[34–38] The $RuO_2(100)$ surface was modelled by the $p(1 \times 3)$ unit cell in a seven-layered slab with 21 Ru atoms and 42 O atoms with a height of 30 Å and the cut-off energy was set to 450 eV. The bottom 9 Ru atoms and 18 O atoms were fixed during geometry optimization processes. A $4 \times 2 \times 1$ Monkhorst–Pack *k*-point sampling was used. The surface models of $RuO_2(100)$ are displayed in Fig. 1 from top and side views. The transition states were localized using a constrained minimization approach with the convergence of forces being 0.05 eV $Å^{-1}$.[39–41] For modelling the aqueous $RuO_2(100)$ interface, 12 explicit interfacial water molecules were set as shown in Fig. 1c. According to the previous work about influence from the number of water layers, the first solvation shell plays the most important role for calculating the reaction energy.[31,32] Here, in our model, 12 explicit water molecules could already form three water layers above the surface that can describe the energy appropriately.

In all the MD simulations, the $RuO_2(100)$ surface and adsorbed species were fixed. In the simulation of the initial water layer structure, the running time of MD simulations was extended to 20 ps until the water structure was relatively stable. Since the water interfacial structures for the initial, transition and final states may be different, the water molecules were running *ab initio* molecular dynamics (MD) for 6 ps (0.5 fs per step, 300 K) for each initial, transition and final state, respectively. The MD simulations were performed at 300 K, and 6 ps time was thus necessary for reaching equilibrium. Using a higher temperature, the simulation time could be reduced. For each state in MD simulations, at least five samples were optimized and the most stable one was used.[31–33] This method has been reported and its accuracy has been tested in the previous work.[32] In the calculation of adsorption energy at the aqueous interface, the adsorption energy was defined as: $E_{ad,aq} = E(ad/surf, aq) - E(ad) - E(surf, aq)$, in which the water competitive adsorption was taken into account.

The $RuO_2(100)$ surface exposes three kinds of surface atoms as illustrated in Fig. 1a: the bridging oxygen (O_{br}) atoms coordinated

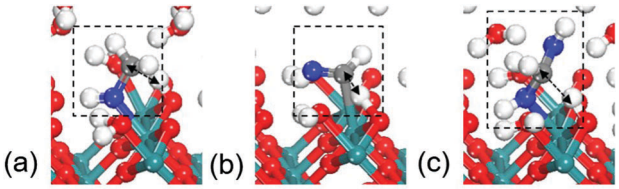

Fig. 2 Transition states for C–H bond breaking in (a) CH_3OH^*, (b) $HCHO^*$ and (c) $HCH(OH)_2^*$. Grey: C; blue: O in C1 intermediates. (The same colors are used in the paper.)

to two Ru atoms with the Ru–O bond length of 1.94 Å, the one-fold under-coordinated Ru ($Ru_{1f\text{-}cus}$) atoms bonded to five O atoms, and the three-fold coordinated oxygen (O_{3c}) atoms bonded to three Ru atoms. At the aqueous $RuO_2(100)$ interface, CH_3OH^* has an adsorption energy of −0.33 eV *via* the O–Ru bond with a distance of 2.13 Å. Since CH_3OH^* could be activated *via* C–H bond or O–H bond pathways with the formation of CH_2OH^* or CH_3O^*,[20] we have examined the two pathways respectively. In the C–H bond dissociation pathway, $CH_3OH^* \rightarrow CH_2OH^* + H^*$, the barrier is as high as 1.40 eV. The C–H bond length is 1.60 Å at the transition state, as shown in Fig. 2a. Such a large barrier suggests that there is little possibility for direct C–H bond activation in CH_3OH^* to take place at room temperature. On the other hand, CH_3OH^* activation *via* the O–H bond as reaction (1) is found to be favourable with the reaction energy of 0 eV and a tiny barrier of 0.09 eV (TS1) for transferring the hydroxyl H to one near an O_{br} atom. The C–H bond breaking in CH_3O^* is easier than that in CH_3OH^*. The barrier is reduced to 0.57 eV with the C–H bond length being 1.33 Å at the TS2 and the formation of formaldehyde ($HCHO^*$) is exothermic by −0.57 eV in reaction (2). These findings indicate that the O–H bond breaking in CH_3OH^* could activate the C–H bond effectively. The energy profile and the structures of intermediates and transition states in $HCHO^*$ formation are presented in Fig. 3. All the calculated data can be found in Table S1 (ESI†).

$$CH_3OH^* \rightarrow CH_3O^* + H^* \quad (1)$$

$$CH_3O^* \rightarrow HCHO^* + H^* \quad (2)$$

It is noteworthy that the C–H bond breaking barrier is calculated on the clean surface without H* from O–H bond cleavage. However, we find that in the presence of H*, the barrier associated with C–H bond breaking in reaction (1) was increased from 0.57 eV to 0.82 eV. This indicates that, the produced H* from methanol should be removed from surface as soon as possible; otherwise it will give rise to a low activity for dehydrogenation. We thus further calculated the H desorption potential, according to the reaction, $H^* \rightarrow H^+ + e^-$, where the free energy of $H^+ + e^-$ can be replaced by that of 1/2 H_2, under SHE conditions.[31] The results show that H* will desorb into solution at 0.84 V (*vs.* SHE), suggestive of a clean $RuO_2(100)$ surface. Since the experimental working potential of methanol electrooxidation is about 1 V, H* produced from methanol dissociation under this condition can be readily transferred into solution as a complete catalytic reaction cycle.

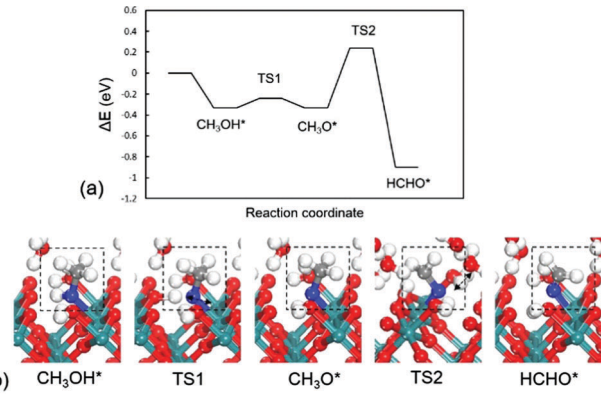

Fig. 3 (a) Energy profile and (b) optimized structures of intermediates and transition states for CH_3OH^* oxidation to HCHO*. TS1: $CH_3OH^* \rightarrow CH_3O^*$; TS2: $CH_3O^* \rightarrow$ HCHO*.

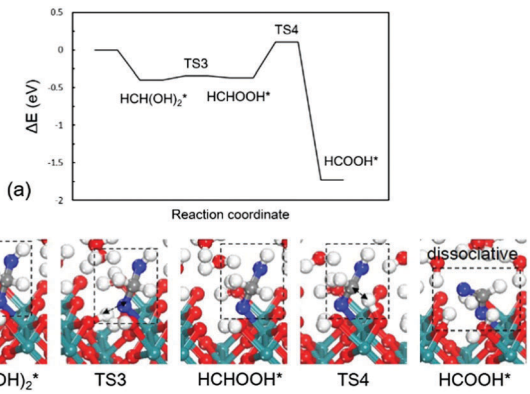

Fig. 4 (a) Energy profile and (b) optimized structures of intermediates and transition for $HCH(OH)_2^*$ oxidation to HCOOH*. TS3: $HCH(OH)_2^* \rightarrow$ HCHOOH*; TS4: HCHOOH* → HCOOH*.

Formaldehyde (HCHO*) has a weak adsorption energy of −0.20 eV at the interface and the O–Ru bond is 2.16 Å, indicating that HCHO* prefers to move away from surface. We find that it is difficult for HCHO* to decompose directly *via* the C–H bond due to the high barrier being 1.73 eV. The C–H bond is 1.31 Å at the transition state as shown in Fig. 2b. The previous experiments and DFT modelling on RuO_2(110) also have shown that further oxidation of formaldehyde is unlikely and HCHO* would desorb into the gas phase,[19] which is in agreement with our results that direct HCHO* decomposition is difficult. However, we note that, since the reactions occur under an aqueous environment, the abundance of interfacial water molecules may open a possible pathway to activate HCHO*. Because of the weak adsorption of HCHO*, a sufficient amount of HCHO* in aqueous solution would be hydrated. HCHO* is found to be active and is easily hydrated to form $HCH(OH)_2^*$ as reaction (3) with a large equilibrium constant in aqueous solution. We have calculated this step in aqueous solution including 32 water molecules. The computational details can be seen in the ESI.† The hydration of HCHO is highly exothermic by −0.94 eV with a slight barrier of 0.1 eV, indicative of a very easy step. Previous calculations have confirmed this path in acetaldehyde electrooxidation.[31] The calculated results reveal that the reactive intermediate for following reactions is indeed $HCH(OH)_2^*$ instead of HCHO*.

$$HCHO^* + H_2O \rightarrow HCH(OH)_2^* \quad (3)$$

The adsorption energy of $HCH(OH)_2$ is −0.41 eV. The optimized configuration is one OH group bonded to the Ru site and the other OH group points upwards being stabilized by the water molecules. Since the molecular geometry of $HCH(OH)_2^*$ is similar to CH_3OH^* with one OH group replacing one H, the oxidation mechanism of $HCH(OH)_2^*$ is similar to that of CH_3OH^*. The energy profile and the structures of intermediates and transition states in $HCH(OH)_2^*$ oxidation to HCOOH* are presented in Fig. 4. Specifically, the dissociation of OH group firstly occurs forming HCHOOH* with a tiny barrier of 0.06 eV for transferring H to O_{br} as reaction (4). The O–H bond distance is elongated to 1.20 Å at the TS3 from the initial 0.99 Å. Then, HCHOOH* easily breaks the C–H bond forming HCOOH* with the barrier of 0.47 eV. The C–H bond length is 1.31 Å at the TS4. The reaction (5) is highly exothermic with a barrier of −1.37 eV. The direct C–H bond activation of $HCH(OH)_2^*$ hardly takes place due to the barrier being as high as 1.16 eV in the reaction, $HCH(OH)_2^* \rightarrow HC(OH)_2^* + H^*$, and the transition state is shown in Fig. 2c.

$$HCH(OH)_2^* \rightarrow HCHOOH^* + H^* \quad (4)$$

$$HCHOOH^* \rightarrow HCOOH^* + H^* \quad (5)$$

HCOOH* at the water/RuO_2(100) interface prefers to dissociatively adsorb on the Ru site without a distinct barrier in reaction (6). Two possible configurations of the adsorbed formate (HCOO*) are compared, *i.e.*, mono-dentate (mono-HCOO*) and bi-dentate (bi-HCOO*). In mono-HCOO*, one O atom is bonded to the Ru site and the other O atom points upwards while in bi-HCOO*, two O atoms are both bonded to two neighbouring Ru sites, as shown in Fig. 5b. Mono-HCOO* is more stable than bi-HCOO* by 0.32 eV: the bare O atom forms several hydrogen bonds with water molecules for stabilizing mono-HCOO*. Not only the higher stability, but also the higher activity of mono-HCOO* than bi-HCOO* for CO_2 formation, indicating that mono-HCOO* is the reactive intermediate. The C–H bond breaking barrier is calculated to be 0.54 eV, which is close to those in CH_3O^* (0.57 eV) and HCHOO* (0.47 eV), but the C–H bond breaking barrier in bi-HCOO* is 1.10 eV. The C–H bond length is 1.38 Å at the TS5 and 1.29 Å at the TS6. Once the C–H bond is broken as reaction (7), the newly formed linear CO_2^* would desorb into solution immediately because of a very weak adsorption energy being only −0.14 eV. The energy profile for HCOOH* oxidation to CO_2^* and the structures of intermediates and transition states are presented in Fig. 5.

$$HCOOH^* \rightarrow \text{mono-HCOO}^* + H^* \quad (6)$$

$$\text{mono-HCOO}^* \rightarrow CO_2^* + H^* \quad (7)$$

The dehydrogenation mechanism on RuO_2(100) differs from that on metal surfaces following a step-wise dehydrogenation mechanism resulting in inevitable CO formation.[18,20–24] On the RuO_2 surface, an indirect C–H bond breaking mechanism is suggested that the O–H bond breaking can effectively lower the C–H bond breaking barriers. On the OH* covered palladium

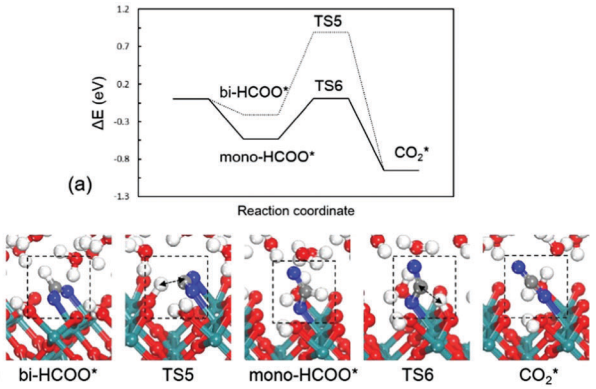

Fig. 5 (a) Energy profile and (b) optimized structures of intermediates and transition states for HCOOH* oxidation to CO_2*. TS5: bi-HCOO* → CO_2*; TS6: mono-HCOO* → CO_2*.

surface, a concerted-like mechanism has been reported that the C–H bond breaking can induce the O–H bond breaking in ethanol, implying an inherent relationship between the C–H and O–H bonds.[31] In experiments for methanol oxidation on RuO_2(100), a plausible mechanism taking COOH* as the unknown intermediate for accounting for the no observation of CO is $CH_3OH^* \rightarrow CH_2OH^* \rightarrow CHOH^* \rightarrow HCOOH^* \rightarrow COOH^* \rightarrow CO_2^*$.[11–13] However, our calculations clearly show evidence that the formation of CH_2OH* and COOH* is not probable, owing to the high barriers in the direct C–H bond dissociations of CH_3OH* and HCOOH*. The overall mechanisms are summarized as: $CH_3OH^* \rightarrow CH_3O^* \rightarrow HCHO^* \rightarrow HCH(OH)_2^* \rightarrow HCHOOH^* \rightarrow HCOOH^* \rightarrow$ mono-$HCOO^* \rightarrow CO_2^*$. The disappearance of CO from *in situ* FTIR spectroscopy should be attributed to the blocking of the further decomposition of HCHO* to CO*,[11–13] suggesting that the formation of CO_2 does not come from CO oxidation but from formic acid decomposition.

For adsorption processes, the presence of an aqueous environment decreases the adsorption energy of surface species significantly due to the competitive water adsorption at the same Ru site. The calculated adsorption energies in the presence and absence of an aqueous environment are listed in Table S2 (ESI†). The presence of hydrogen bonds between adsorbates and water molecules can also affect the binding energy, in particular for HCOO*. In a vacuum, bi-HCOO* is more stable thermodynamically than mono-HCOO* by 0.84 eV since the two bare O atoms in HCOO* prefer to occupy two neighbouring Ru sites. However, the aqueous environment stabilizes mono-HCOO* by 0.32 eV *via* hydrogen bonding between one dangling O atom and water molecules, as shown in Fig. 5b. Bader charge analysis in Table S3 (ESI†) shows that the charges in surface species are not affected by water noticeably. CH_3O* and bi-HCOO* are more negatively charged by −0.02 *e* and −0.04 *e* respectively. −0.12 *e* is transferred to HCHOO* and −0.17 *e* is transferred from surface to mono-HCOO*. In general, water influence on the thermodynamics is significant but on the kinetics is not. Note that, the interfacial water structure plays a critical role in determining binding energies by coverage, competitive adsorption and hydrogen bonding. Here, we mainly focused on and reported the binding energies.

In summary, some insights into the methanol oxidation at the aqueous RuO_2(100) interface have been gained by combining first principles calculations and *ab initio* MD simulations. The methanol oxidation mechanisms have been identified as: $CH_3OH^* \rightarrow CH_3O^* \rightarrow HCHO^* \rightarrow HCH(OH)_2^* \rightarrow HCHOOH^* \rightarrow HCOOH^* \rightarrow$ mono-$HCOO^* \rightarrow CO_2^*$, which is very different from that on metal surfaces where CO formation is inevitable. The coupling between HCHO* and one water molecular forming $HCH(OH)_2$* is the key step for the following reactions. Aqueous environment is found to stabilize mono-HCOO* effectively *via* hydrogen bonding between the dangling O atom and water molecules, making the higher stability and activity of mono-HCOO* than bi-HCOO* for CO_2 formation. This theoretical study of C1 molecules would help understand the catalytic process of other small organic molecules on metal oxide surfaces.

This work is supported by NSFC (21361140374, 21321062 and 21573183) and EPSRC (EP/I013229/1).

Notes and references

1 T. Iwasita, *Electrochim. Acta*, 2002, **47**, 3663.
2 S. G. Sun and J. Clavilier, *J. Electroanal. Chem.*, 1987, **236**, 95.
3 E. Herrero, K. Franaszczuk and A. Wieckowski, *J. Phys. Chem.*, 1994, **98**, 5074.
4 H. A. Gasteiger, N. Markovic, P. N. Ross and E. J. Cairns, *J. Phys. Chem.*, 1993, **97**, 12020.
5 W. Chrzanowski and A. Wieckowski, *Langmuir*, 1998, **14**, 1967.
6 M. Watanabe and S. Motoo, *J. Electroanal. Chem. Interfacial Electrochem.*, 1975, **60**, 267.
7 T. Frelink, W. Visscher and J. A. R. van Veen, *Surf. Sci.*, 1995, **335**, 353.
8 D. J. Chen and Y. Y. J. Tong, *Angew. Chem., Int. Ed.*, 2015, **54**, 9394.
9 H. Over, *Chem. Rev.*, 2012, **112**, 3356.
10 H. Over, Y. D. Kim, A. P. Seitsonen, S. Wendt, E. Lundgren, M. Schmid, P. Varga, A. Morgante and G. Ertl, *Science*, 2000, **287**, 1474–1476.
11 W. F. Lin, P. A. Christensen and A. Hamnett, *Phys. Chem. Chem. Phys.*, 2001, **3**, 3312.
12 W. F. Lin, J. M. Jin, P. A. Christensen and K. Scott, *Electrochim. Acta*, 2003, **48**, 3815.
13 W. F. Lin and P. A. Christensen, *Faraday Discuss.*, 2002, **121**, 267.
14 W. F. Lin, M. S. Zei, Y. D. Kim, H. Over and G. Ertl, *J. Phys. Chem. B*, 2000, **104**, 6040.
15 B. Y. Liu, J. M. Jin, C. Hardacre, P. Hu and W. F. Lin, *J. Electroanal. Chem.*, 2013, **688**, 216.
16 W. B. Wang, M. S. Zei and G. Ertl, *Chem. Phys. Lett.*, 2002, **355**, 301.
17 Y. H. Fang and Z. P. Liu, *J. Am. Chem. Soc.*, 2010, **132**, 18214.
18 X. Lu, W. Wang, Z. Deng, H. Zhu, S. Wei, S. P. Ng, W. Guo and C. M. L. Wu, *RSC Adv.*, 2015, **6**, 1729.
19 N. Lopez and G. Novell-Leruth, *Phys. Chem. Chem. Phys.*, 2010, **12**, 12217.
20 C. J. Zhang and P. Hu, *J. Chem. Phys.*, 2001, **115**, 7182.

21 S. K. Desai, M. Neurock and K. Kourtakis, *J. Phys. Chem. B*, 2002, **106**, 2559.
22 J. Greeley and M. Mavrikakis, *J. Am. Chem. Soc.*, 2002, **124**, 7193.
23 T. Sheng, X. Lin, Z. Y. Chen, P. Hu, S. G. Sun, Y. Q. Chu, C. A. Ma and W. F. Lin, *Phys. Chem. Chem. Phys.*, 2015, **17**, 25235.
24 T. Sheng and S. G. Sun, *J. Electroanal. Chem.*, 2016, **781**, 24.
25 C. D. Taylor, S. A. Wasileski, J. S. Filhol and M. Neurock, *Phys. Rev. B: Condens. Matter Mater. Phys.*, 2006, **73**, 165402.
26 M. Otani, I. Hamada, O. Sugino, Y. Morikawa, Y. Okamoto and T. Ikeshoji, *Phys. Chem. Chem. Phys.*, 2008, **10**, 3609.
27 E. Skulason, G. S. Karlberg, J. Rossmeisl, T. Bligaard, J. Greeley, H. Josson and J. K. Norskov, *Phys. Chem. Chem. Phys.*, 2007, **9**, 3241–3250.
28 Y. H. Fang, G. F. Wei and Z. P. Liu, *Catal. Today*, 2013, **202**, 98.
29 T. Sheng, D. Wang, W. F. Lin, P. Hu and S. G. Sun, *Electrochim. Acta*, 2016, **190**, 446.
30 T. Sheng, W. F. Lin and S. G. Sun, *Phys. Chem. Chem. Phys.*, 2016, **18**, 15304.
31 T. Sheng, W. F. Lin, C. Hardacre and P. Hu, *J. Phys. Chem. C*, 2014, **118**, 5762.
32 J. Liu, X. M. Cao and P. Hu, *Phys. Chem. Chem. Phys.*, 2014, **16**, 4176.
33 L. Yu, X. L. Pan, X. M. Cao, P. Hu and X. H. Bao, *J. Catal.*, 2011, **282**, 183.
34 G. Kresse and J. Hafner, *Phys. Rev. B: Condens. Matter Mater. Phys.*, 1993, **48**, 13115.
35 G. Kresse and J. Furthmuler, *Phys. Rev. B: Condens. Matter Mater. Phys.*, 1996, **54**, 11169.
36 P. E. Blochl, *Phys. Rev. B: Condens. Matter Mater. Phys.*, 1994, **50**, 17953.
37 G. Kresse and D. Joubert, *Phys. Rev. B: Condens. Matter Mater. Phys.*, 1999, **59**, 1758.
38 J. P. Pedrew, K. Burke and M. Ernzerhof, *Phys. Rev. Lett.*, 1996, **77**, 3865.
39 A. Alavi, P. Hu, T. Deutsch, P. L. Silvestrelli and J. Hutter, *Phys. Rev. Lett.*, 1998, **80**, 3650.
40 A. Michaelides, Z. P. Liu, C. J. Zhang, A. Alavi, D. A. King and P. Hu, *J. Am. Chem. Soc.*, 2003, **125**, 3704.
41 Z. P. Liu and P. Hu, *J. Am. Chem. Soc.*, 2003, **125**, 1958.

